INTERNATIONAL JOURNAL FOR NUMERICAL METHODS IN FLUIDS, VOL. 9, 193–212 (1989)

EFFECTS OF GRID STAGGERING ON NUMERICAL SCHEMES

T. M. SHIH AND C. H. TAN

Department of Mechanical Engineering, University of Maryland, College Park, MD 20742, U.S.A.

AND

B. C. HWANG

David Taylor Research Center, Annapolis, MD 21402, U.S.A.

SUMMARY

Nine finite difference schemes using primitive variables on various grid arrangements were systematically tested on a benchmark problem of two-dimensional incompressible Navier–Stokes flows. The chosen problem is similar to the classical lid-driven cavity flow, but has a known exact solution. Also, it offers the reader an opportunity to thoroughly evaluate accuracies of various conceptual grid arrangements.

Compared to the exact solution, the non-staggered grid scheme with higher-order accuracy was found to yield an accuracy significantly better than others. In terms of 'overall performance', the so-called 4/1 staggered grid scheme proved to be the best. The simplicity of this scheme is the primary benefit. Furthermore, the scheme can be changed into a non-staggered grid if the pressure is replaced by the pressure gradient as a field variable.

Finally, the conventional staggered grid scheme developed by Harlow and Welch also yields relatively high accuracy and demonstrates satisfactory overall performance.

KEY WORDS Navier–Stokes Staggered grid Primitive variable formulation

1. INTRODUCTION

Two types of grid layout can be applied to the primitive variable finite difference method that solves incompressible Navier–Stokes flows—staggered grids[1–4] and non-staggered grids.[5,6] In finite element terminology, staggered grids are similar to mixed-order interpolation functions;[7,8] non-staggered grids resemble same-order interpolation functions.[9]

While a non-staggered grid appears simple and natural, it leads to algebraic systems with singular coefficient matrices that contain too many zero eigenvalues. Consequently, the resulting pressure solution is contaminated with pressure modes and is grossly erroneous. To avoid this problem, researchers began adopting staggered grids in which the nodal velocity components and the pressure are placed in different locations. For flows with small convection, the staggered grid solution also appears to be more accurate than the non-staggered grid result.

The computer programming for staggered grids appears to be more complex than for non-staggered grids because each velocity component requires different indexing. Furthermore, the computation of the convection terms, $\partial(uv)/\partial x$ or $\partial(uv)/\partial y$, may become inaccurate for large Reynolds numbers because the velocity components are staggered. It may be worthwhile to

0271-2091/89/020193-20$10.00

Received 15 December 1987
Revised 27 April 1988

reconsider the use of non-staggered grids, unless the accuracy and convergence rate of numerical schemes using staggered grids prove to be significantly better, or unless the pressure solution is of primary interest.

The objectives of this paper are: (1) to use nine numerical schemes (five staggered grids and four non-staggered grids) to solve a benchmark problem, and to compare the computed and exact solutions; (2) to identify the shortcomings and merits of each scheme; and (3) to recommend a scheme, based on the accuracy and the overall performance.

A well known benchmark problem is the lid-driven cavity flow originated by Burggraf.[10] Some researchers, including the authors of this paper, are unsure of the singularity at the two corners where the moving lid remains in contact with the stationary walls. They have found that specification of the velocity of either unity or zero at the two corners alters the numerical result.

Furthermore, it is difficult to compare the details of nodal values precisely, because the benchmark solution generally is presented in graphic form. Even if a tabulated benchmark solution is available, transferring it into the computer program to compute the global errors would prove laborious.

Therefore we propose a benchmark problem similar to the classical lid-driven cavity flow. The flow velocity at the two corners is now zero; the flow is driven by a specified body force (as described in the next section) in addition to a non-uniform shear. Most importantly, the exact solution to this problem exists and is known.

2. CONTINUUM EQUATIONS GOVERNING THE BENCHMARK PROBLEM

Illustrated in Figure 1, the recirculating cavity flow driven by combined shear and body forces is governed by

$$\nabla \cdot \mathbf{u} = 0, \tag{1}$$

$$\mathbf{u} \cdot \nabla u = \frac{1}{Re} \nabla^2 u - \frac{\partial p}{\partial x} \tag{2}$$

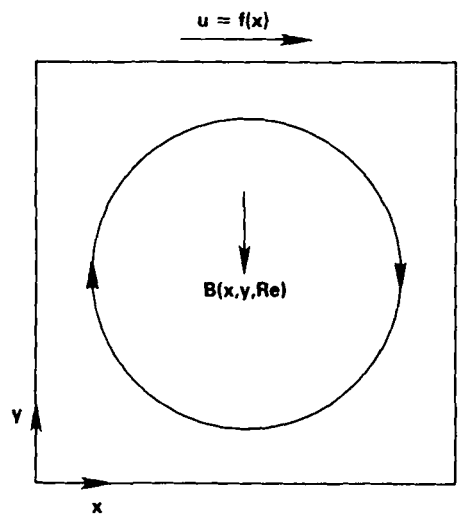

Figure 1. System schematic of the benchmark problem

and

$$\mathbf{u}\cdot\nabla v=\frac{1}{Re}\nabla^2 v-\frac{\partial p}{\partial y}-B(x,\ y,\ Re). \tag{3}$$

The boundary conditions for the velocities u and v are of Dirichlet type: zero everywhere except along the top surface where

$$u(x,\ 1)=16(x^4-2x^3+x^2). \tag{4}$$

Equation (4) also indicates that $u(0,\ 1)=0$ and $u(1,\ 1)=0$, which eliminates the ambiguity of specifying the top corner velocities as in the classical lid-driven flow problem.

A body force is present in the y-direction and is prescribed as

$$B(x,\ y,\ Re)=-\frac{8}{Re}[24F(x)+2f'(x)g''(y)+f'''(x)g(y)]-64[F_2(x)G_1(y)-g(y)g'(y)F_1(x)], \tag{5}$$

where

$$\begin{aligned}
&f(x)=x^4-2x^3+x^2,\\
&g(y)=y^4-y^2,\\
&F(x)=\int f(x)\,dx=0{\cdot}2x^5-0{\cdot}5x^4+x^3/3,\\
&F_1(x)=f(x)f''(x)-[f'(x)]^2=-4x^6+12x^5-14x^4+8x^3-2x^2,\\
&F_2(x)=\int f(x)f'(x)\,dx=0{\cdot}5[f(x)]^2,\\
&G_1(y)=g(y)g'''(y)-g'(y)g''(y)=-24y^5+8y^3-4y
\end{aligned}$$

and the primes on $f(x)$ and $g(y)$ denote the differentiation with respect to x and y respectively.

The exact solution to this combined shear- and body-force-driven cavity flow exists and is known to be

$$u(x,\ y)=8f(x)g'(y)=8(x^4-2x^3+x^2)(4y^3-2y), \tag{6a}$$

$$v(x,\ y)=-8f'(x)g(y)=-8(4x^3-6x^2+2x)(y^4-y^2) \tag{6b}$$

and

$$p(x,\ y,\ Re)=\frac{8}{Re}[F(x)g'''(y)+f'(x)g'(y)]+64F_2(x)\{g(y)g''(y)-[g'(y)]^2\}. \tag{6c}$$

For convenience, the exact solution of $u(x,\ y)$, $v(x,\ y)$ and $\partial p/\partial y$ for $Re=1$ is displayed in Table I corresponding to the physical location in the flow field. The corresponding streamlines are plotted in Figure 2. It is observed that, qualitatively, the clockwise circulation is similar to the classical lid-driven recirculating flow.

An additional inconvenience of the present benchmark problem is the need to include the lengthy source term expression in the v-momentum equation. Readers who intend to solve the benchmark problem may ensure the correctness of the expression in their computer programs by ensuring that $B(0{\cdot}5,\ 0{\cdot}5,\ 1)=-3{\cdot}356250$.

3. NUMERICAL SCHEMES EXAMINED

Nine primitive variable schems are used to solve the benchmark problem. Scheme (b) is a modification of scheme (a), and scheme (e) is a modification of scheme (d); most other schemes

Table I. Exact solution of u, v and $\partial p/\partial y$ to the combined shear- and body-force-driven cavity flow problem

	$i=1$				$u(x, y)$					$i=n+1$
$j=1$	0·0	0·1296	0·4096	0·7056	0·9216	1·0000	0·9216	0·7056	0·4096	0·1296	0·0
	0·0	0·0723	0·2286	0·3937	0·5143	0·5580	0·5143	0·3937	0·2286	0·0723	0·0
	0·0	0·0290	0·0918	0·1581	0·2064	0·2240	0·2064	0·1581	0·0918	0·0290	0·0
	0·0	−0·0018	−0·0057	−0·0099	−0·0129	−0·0140	−0·0129	−0·0099	−0·0057	−0·0018	0·0
	0·0	−0·0218	−0·0688	−0·1185	−0·1548	−0·1680	−0·1548	−0·1185	−0·0688	−0·0218	0·0
	0·0	−0·0324	−0·1024	−0·1764	−0·2304	−0·2500	−0·2304	−0·1764	−0·1024	−0·0324	0·0
	0·0	−0·0353	−0·1114	−0·1919	−0·2507	−0·2720	−0·2507	−0·1919	−0·1114	−0·0353	0·0
	0·0	−0·0319	−0·1008	−0·1736	−0·2267	−0·2460	−0·2267	−0·1736	−0·1008	−0·0319	0·0
	0·0	−0·0238	−0·0754	−0·1298	−0·1696	−0·1840	−0·1696	−0·1298	−0·0754	−0·0238	0·0
	0·0	−0·0127	−0·0401	−0·0691	−0·0903	−0·0980	−0·0903	−0·0691	−0·0401	−0·0127	0·0
$j=n+1$	0·0	0·0000	0·0000	0·0000	0·0000	0·0000	0·0000	0·0000	0·0000	0·0000	0·0
					$v(x, y)$						
	$i=1$									$i=n+1$	
$j=1$	0·0	0·0000	0·0000	0·0000	0·0000	0·0000	0·0000	0·0000	0·0000	0·0000	0·0
	0·0	0·1773	0·2364	0·2068	0·1182	0·0000	−0·1182	−0·2068	−0·2364	−0·1773	0·0
	0·0	0·2654	0·3539	0·3097	0·1769	0·0000	−0·1769	−0·3097	−0·3539	−0·2654	0·0
	0·0	0·2879	0·3838	0·3359	0·1919	0·0000	−0·1919	−0·3359	−0·3838	−0·2879	0·0
	0·0	0·2654	0·3539	0·3097	0·1769	0·0000	−0·1769	−0·3097	−0·3539	−0·2654	0·0
	0·0	0·2160	0·2880	0·2520	0·1440	0·0000	−0·1440	−0·2520	−0·2880	−0·2160	0·0
	0·0	0·1548	0·2064	0·1806	0·1032	0·0000	−0·1032	−0·1806	−0·2064	−0·1548	0·0
	0·0	0·0943	0·1258	0·1101	0·0629	0·0000	−0·0629	−0·1101	−0·1258	−0·0943	0·0
	0·0	0·0442	0·0590	0·0516	0·0295	0·0000	−0·0295	−0·0516	−0·0590	−0·0442	0·0
	0·0	0·0114	0·0152	0·0133	0·0076	0·0000	−0·0076	−0·0133	−0·0152	−0·0114	0·0
$j=n+1$	0·0	0·0000	0·0000	0·0000	0·0000	0·0000	0·0000	0·0000	0·0000	0·0000	0·0
					$\partial p/\partial y$						
		$i=2$								$i=n$	
$j=2$		8·0569	8·4727	5·7580	3·7352	3·2000	2·6648	0·6421	−2·0726	−1·6573	
		6·0780	6·9031	5·3735	3·9278	3·2000	2·4722	1·0265	−0·5031	0·3218	
		4·2193	5·0439	4·3193	3·5641	3·2000	2·8358	2·0808	1·3562	2·1806	
		2·5379	3·1357	2·9583	2·9151	3·2000	3·4849	3·4418	3·2643	3·8620	
		1·0761	1·3562	1·5579	2·1803	3·2000	4·2197	4·8421	5·0438	5·3238	
		−0·1369	−0·1718	0·3038	1·4982	3·2000	4·9018	6·0962	6·5718	6·5369	
		−1·0829	−1·3703	−0·6870	0·9562	3·2000	5·4438	7·0870	7·7703	7·4828	
		−1·7518	−2·1980	−1·3518	0·6011	3·2000	5·7939	7·7518	8·5980	8·1517	
$j=n$		−2·1403	−2·6404	−1·6690	0·4490	3·2000	5·9510	8·0690	9·0404	8·5402	

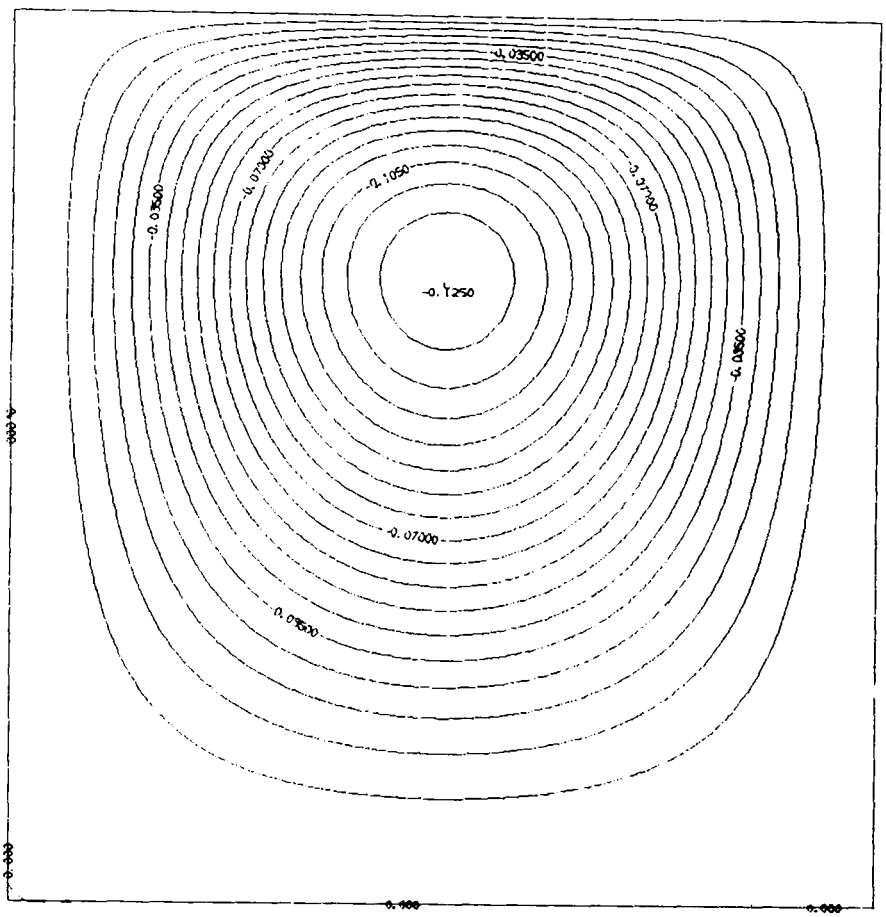

Figure 2. Streamlines of the flow

have been frequently or occasionally used by other researchers. Their grid arrangements for a 2D square computational domain will be described and are shown graphically in Figure 3. The symbol m/n is used in the names of these schemes, where m is the number of u or v unknowns in a square cell and n designates the number of p unknowns. The control volumes for mass conservation and u-momentum conservation are the squares that are shaded diagonally and horizontally respectively. In Figures 3(a) and 3(b) the control volumes for v-momentum conservation enclose nodes for v.

(*a*) 2/1 *staggered grid* (*Harlow and Welch*[1])

In Figure 3(a) p is located at the centre of the square element. Due to grid staggering, u is located a half grid from the top surface and the bottom wall, suggesting that a special treatment is required to compute us that are adjacent to the top and bottom boundaries. One way is to extrapolate u_a, u_b and u_c to obtain u_i, which is located beyond the computational domain. A similar situation arises for the vs.

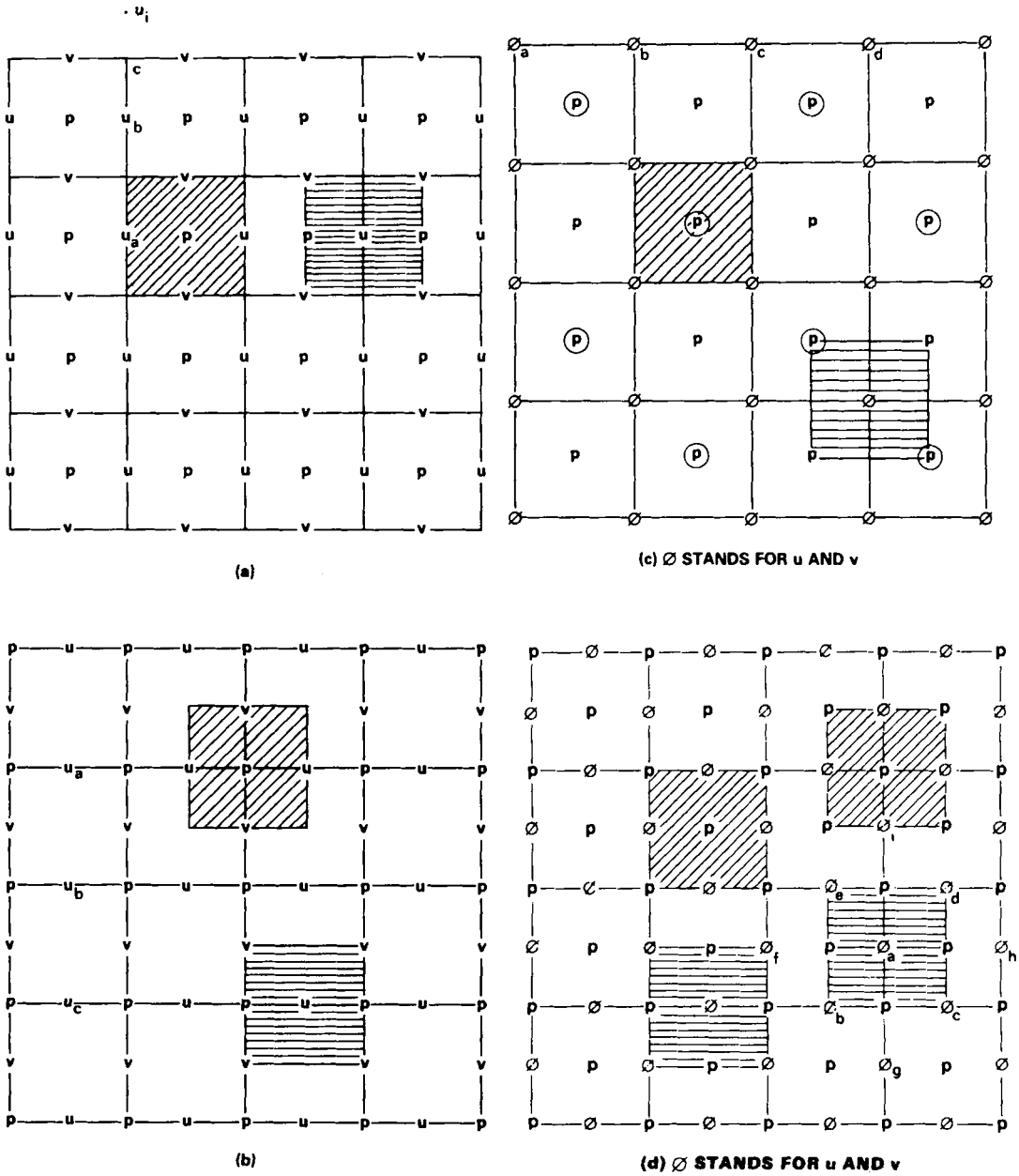

Figure 3 (a–d)

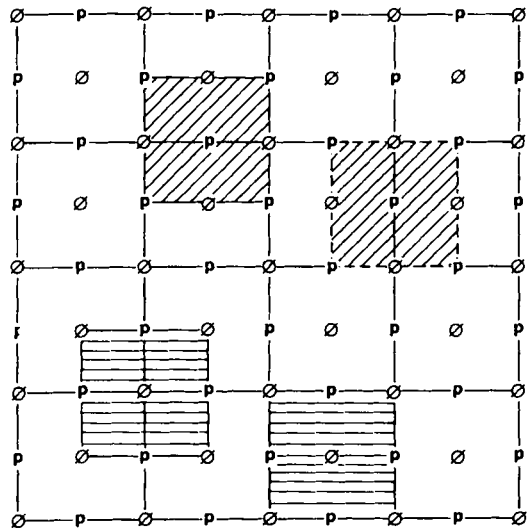

(e) Ø STANDS FOR u AND v

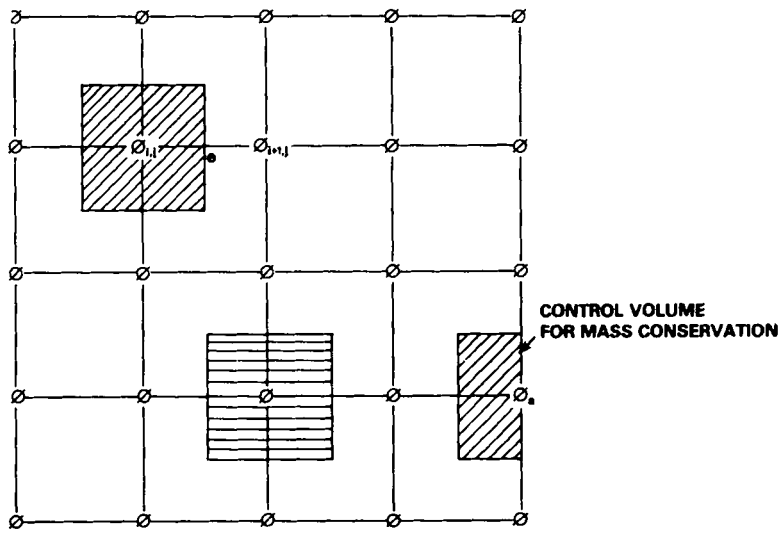

(f) Ø STANDS FOR u, v, AND p

Figure 3 (e–f)

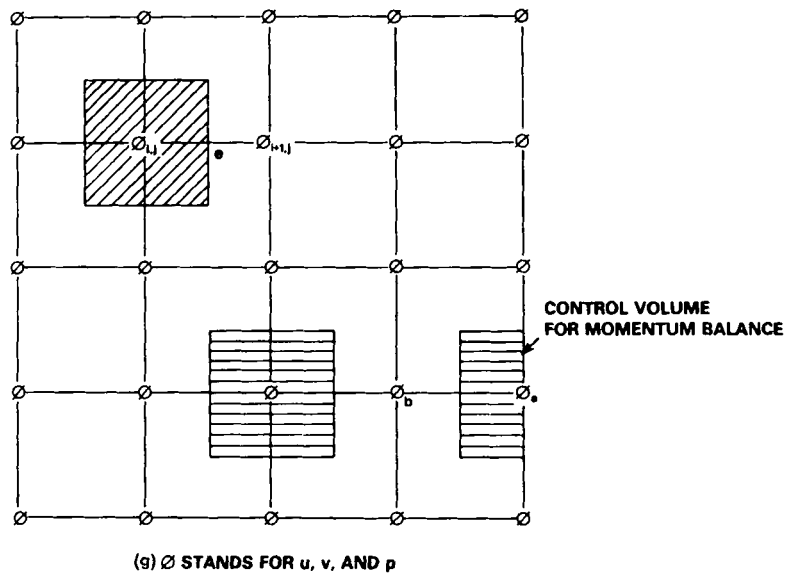

Figure 3. Grid arrangement for nine various primitive variable schemes, which are identified by m/n where m is the number of u or v unknowns in the square cell and n is that of p unknowns. (a) 2/1 staggered grid. (b) 2/4 staggered grid. (c) 4/1 staggered grid; ϕ denotes u or v. (d) 4/5 staggered grid; ϕ denotes u or v. (e) 5/4 staggered grid; ϕ denotes u or v. (f) 4/4 non-staggered grid with the continuity equation used to compute the boundary pressure; ϕ denotes u, v or p. (g) 4/4 non-staggered grid with the momentum equation used to compute the boundary pressure; ϕ denotes u, v or p

(*b*) 2/4 *staggered grid* (*modification of* (*a*))

In Figure 3(b) p is located at the grid node; u is located a half grid interval from the left and right walls; and v is located a half grid interval from the bottom and top walls. While the modification appears almost trivial, it makes extrapolation unnecessary because the us and vs adjacent to the vertical boundary (such as u_a , u_b and u_c) can be computed directly from the continuity equation. Thus it is not necessary to compute the boundary pressure either.

(*c*) 4/1 *staggered grid*

Figure 3(c) shows a partially staggered grid with only the presssure staggered to the centre of the square element.[11-17] The velocity components u and v are located at the same positions.

(*d*) 4/5 *staggered grid*

Figure 3(d) results from superimposing Figures 3(a) and 3(b).[18] Therefore the computational domain will be covered twice if all the control volumes for the mass conservation are drawn. Now all us and vs are located at the same positions.

(*e*) 5/4 *staggered grid* (*modification of* (*d*))

In Figure 3(e) the us and vs are located at the four corners and at the centre of the element; the ps are located at the midpoint of the four sides of the element.

(*f*) 4/4 *non-staggered grid* (*with the continuity equation applied on the boundary to compute p there*)

In Figure 3(f) all us, vs and ps are located at the grid points.[5,6] The velocities and pressures on the face of the control volume are taken to be the average of the two adjacent nodal unknowns. For example, u_e is $(u(i-1, j)+u(i, j))/2$ and p_e is $(p(i-1, j)+p(i, j))/2$.

In this formulation the pressure on the boundary (e.g. P_a) is computed by balancing the mass over the rectangular control volume, half the size of the regular control volume.

(*g*) 4/4 *non-staggered grid* (*with the momentum equation applied on the boundary to compute p there*)

This formulation is the same as that in (f) except that now the pressure on the boundary is computed by balancing the momentum over the rectangular control volume.[5] This should enhance the link between two adjacent nodal pressures.

(*h*) 4/4 *non-staggered grid* (*pressure Poisson equation*)[1,19,20]

In this formulation the pressure is computed by using the pressure Poisson equation

$$\nabla^2 p = \frac{1}{Re}\nabla^2\left(\frac{\partial u}{\partial x}+\frac{\partial v}{\partial y}\right)-\frac{\partial}{\partial x}(\mathbf{u}\cdot\nabla u)-\frac{\partial}{\partial y}(\mathbf{u}\cdot\nabla v) \tag{7}$$

instead of using the continuity equation as in schemes (f) and (g). However, to ensure a divergence-free solution, we need to use the continuity equation, not the momentum equation, to compute p on the boundary. This remark is explained further in Section 5.

(*i*) 4/4 *non-staggered grid* (*higher-order formulation*)

In schemes (f) and (g) the accuracy may be lowered and spurious numerical oscillation may be generated when the velocities and pressures on the face of the control volume are approximated by the average values of the two adjacent nodal unknowns. The accuracy may be increased and the oscillation problem may be eliminated if the first derivatives $\partial u/\partial x$, $\partial v/\partial y$, $\partial p/\partial x$ and $\partial p/\partial y$ are treated as additional unknowns, and if additional equations are derived to compute these variables. These additional equations, according to the 'Pade' formulation, are

$$m_{i-1}+4m_i+m_{i+1}=\frac{3}{h}(\phi_{i+1}-\phi_{i-1}),$$

where ϕ denotes u, v or p, and m denotes their respective derivatives. The boundary condition of m is approximated by a five-point one-sided relation as

$$m_1=\frac{1}{12h}(-25\phi_1+48\phi_2-36\phi_3+16\phi_4-3\phi_5)+O(h^4).$$

4. NUMERICAL PROCEDURES AND NUMERICAL SOLUTIONS

To conduct a fair comparison of various grid networks, we adopt a series of conventional procedures for our computations: (a) Gauss–Seidel point-by-point iterative method; (b) central finite difference; (c) under-relaxation; and (d) a modified penalty function method to solve for p, which is described as follows.

The continuity equation is modified into

$$\lambda p+(1-\lambda)\nabla\cdot\mathbf{u}=0 \tag{8a}$$

or

$$p = -\frac{1-\lambda}{\lambda}\nabla \cdot \mathbf{u}. \tag{8b}$$

The procedure starts from $\lambda = 1$ when the pressure is zero throughout the flow field. Gradually, λ is reduced from 1 to, say, 0·5. The solution at $\lambda = 1$ is used as the starting guess for that at $\lambda = 0{\cdot}5$. The procedure is repeated successively for $\lambda = 0{\cdot}1$, 0·05, 0·01, 0·005, 0·001, 0·0005, 0·0001, 0·00005 and 0·00001. At $\lambda = 0{\cdot}00001$, $\nabla \cdot \mathbf{u}$ becomes very small, but p remains finite and is the true numerical solution to the Navier–Stokes equation. Note that this scheme also is similar to the false transient method initiated by Chorin,[21] because p is artificially introduced into the continuity equation. However, unlike the false transient scheme, the present scheme can solve true transient problems also, because the variable is λ, not t.[22]

All of the schemes are programmed along the following logical path.

(1) Specify data such as Re, h and the convergence criteria; define the functions $f(x)$, $g(y)$, etc.; and compute the body force $B(x, y, Re)$.
(2) Specify the velocity boundary condition. In particular, the flow on the top surface is driven according to equation (4). An outer DO loop for the Gauss–Seidel iteration starts here.
(3) Compute interior us (by an inner DO loop).
(4) Compute interior vs (by an inner DO loop). For non-staggered grids u and v can be conveniently computed in a single DO loop because the same indices i and j are applicable to both $u(i, j)$ and $v(i, j)$.
(5) Compute p boundary conditions using equation (8b). This step is not needed for staggered grid schemes (a), (b), (c), (d) and (e). For scheme (g) the momentum equation (applied to the boundary normal to the velocity component) is used.
(6) Compute interior ps (by an inner DO loop). The outer DO loop for the Gauss–Seidel iteration ends here. If the solution has converged, go to (7); if not, go back to (3).
(7) Print the output.

The computer programs of all the schemes are validated by the following debugging procedure.[23] First, we create a simple fictitious problem. The governing equations are

$$\nabla \cdot \mathbf{u} = 0, \tag{9}$$

$$\mathbf{u} \cdot \nabla u = \frac{1}{Re}\nabla^2 u - \frac{\partial p}{\partial x} + g_1(x, y, Re) \tag{10}$$

and

$$\mathbf{u} \cdot \nabla v = \frac{1}{Re}\nabla^2 v - \frac{\partial p}{\partial y} + g_2(x, y, Re), \tag{11}$$

where

$$g_1(x, y, Re) = 4x^3y^2 + 2xy^2 - 4y/Re$$

and

$$g_2(x, y, Re) = 4x^2y^3 + 2x^2y + 4x/Re.$$

The exact solution to equations (9)–(11) exists and is known to be

$$u(x, y) = 2x^2y, \qquad v(x, y) = -2xy^2, \qquad p(x, y) = x^2y^2 \tag{12}$$

if the boundary conditions of u and v are prescribed as

$$u(1, y)=2y, \qquad u(x, 1)=2x^2, \qquad v(1, y)=-2y^2, \qquad v(x, 1)=-2x$$

and zero elsewhere.

We then use all the schemes to solve this problem first. If the program is free of programming errors, the numerical solution should be identical to the exact solution given in equation (12), because the central finite difference approximation is exempt from truncation errors for second-degree polynomials. After the identity is observed, we simply delete $g_1(x, y, Re)$, replace $g_2(x, y, Re)$ with $-B(x, y, Re)$ and change the boundary condition to equation (4).

All the computations are performed on a VAX-785 mainframe with $h=0{\cdot}05$ ($n=20$).

In Table II the shortcomings of the nine schemes are summarized. They are discussed further in the next section.

Table III shows the standard deviation of the nodal variables with respect to the exact solution, defined as

$$e_\phi=\left(\frac{\text{summation of all } [\phi(i, j)-\phi_{\text{exact}}(x, y)]^2}{\text{number of all nodal } \phi\text{s}}\right)^{1/2}, \tag{13}$$

where ϕ stands for u, v or $\partial p/\partial y$. It is unfair to compare p, because p is oscillatory in schemes (c), (d), (e), (f) and (i).

5. DISCUSSION

Computations are performed for $Re=1$ and 10. At $Re=10$ more severe under-relaxation is needed generally to obtain convergent solutions for these central finite different schemes. For flows with

Table II. Shortcomings of the nine schemes. Y, N and N/A denote 'yes', 'no' and 'not applicable' respectively

	Scheme								
Shortcoming	(a)	(b)	(c)	(d)	(e)	(f)	(g)	(h)	(i)
Set of algebraic equations may be inconsistent	N	N	Y	N	N	N	Y	N	N
p is oscillatory	N	N	Y	Y	Y	Y	N	N	Y
Sometimes even pressure gradients are oscillatory	N	N	N	N	N	Y	N	N	N
Computation of p boundary condition is needed	N	N	N	Y	N	Y	Y	Y	Y
Indexing in the computer program is relatively cumbersome	Y	Y	N	Y	Y	N	N	N	N
Extrapolation for fictitious velocity components is needed	Y	N	N	Y	N	N	N	N	N
Averaging of u or v for convection term is needed	Y	Y	N	N	N	N	N	N	N
Pressure gradients will involve us or vs beyond the nine-point stencil	N	N	N	Y	N	Y	Y	N/A	N
CPU time per iteration is relatively large	N	N	N	Y	Y	N	N	N	Y
Mass conservation is generally poor	N	N	N	Y	Y	N	Y	Y	Y
Accuracy of pressure gradients is relatively low	N	Y	N	N	Y	N	N	N	N

Table III. Standard deviation of the nodal u, v and $\partial p/\partial y$ with respect to the exact solution ($n=20$)

Numerical scheme		e_u	e_v	e_{py}
(a)	$Re=1$	0·000777	0·000730	0·086742
2/1 staggered	$Re=10$	0·000780	0·000731	0·010122
(b)	$Re=1$	0·000849	0·000975	0·250820
2/4 staggered	$Re=10$	0·006218	0·007774	0·246650
(c)	$Re=1$	0·001373	0·001769	0·206944
4/1 staggered	$Re=10$	0·001391	0·001788	0·020724
(d)	$Re=1$	0·000777	0·000731	0·086660
4/5 staggered	$Re=10$	0·000781	0·000740	0·009595
(e)	$Re=1$	0·000550	0·000781	2·697950
5/4 staggered	$Re=10$	0·000905	0·000851	0·285976
(f)	$Re=1$	0·002626	0·003044	0·341469
4/4 non-staggered (C)	$Re=10$	0·002640	0·003066	0·035149
(g)	$Re=1$	0·002820	0·003236	0·280579
4/4 non-staggered (M)	$Re=10$	0·002833	0·003257	0·029399
(h)	$Re=1$	0·003659	0·000695	0·183157
4/4 non-staggered (PP)	$Re=10$	0·003697	0·001196	0·019960
(i)	$Re=1$	0·000141	0·000081	0·031432
4/4 non-staggered (HO)	$Re=10$	0·000114	0·000109	0·003035

$Re>10$ it becomes more difficult for the central finite difference solution to converge, and, if convergent at all, the solution appears grossly inaccurate.

Below, we attempt to identify the merits and shortcomings of each scheme.

(a) 2/1 *staggered grid*

This scheme may be the most widely used, possibly because the pressure solution is non-oscillatory. The velocity components are located exactly on the faces of the control volume for the mass conservation; therefore the only linear combination of the discretized continuity equations such that all the interior us and vs vanish is to add up all the continuity equations. The singularity of the resulting coefficient matrix (which has only one zero eigenvalue) corresponds to the so-called hydrostatic pressure mode and leads to an arbitrary, yet unharmful, constant in the pressure solution.

However, three shortcomings have been identified.

(1) The nodal velocities do not lie entirely on the boundary of the computational domain. This suggests that, for computing velocities adjacent to the top and bottom surfaces, some extrapolation may be needed to first compute imaginary nodal us located beyond the computational domain. The accuracy may be lowered if too few nodes are used in the extrapolation. Conversely, too many nodes may reduce the convergence rate. A similar situation arises for the vs.

(2) Since the us and vs are staggered at different locations, we must assume that either the u value (when computing v) or the v value (when computing u) in the convection term $\partial(uv)/\partial x$

or $\partial(uv)/\partial y$ is the average of its neighbouring four values. This averaging process may lower the accuracy significantly when the velocity gradients are large.

(3) The computer programming involves different indexing for u, v and p.

(b) 2/4 *staggered grid* (*slight modification of* (a))

As in (a), the strong merit of this scheme is the non-oscillatory pressure. The major difference between (a) and (b) is that the us are staggered from the top and bottom boundaries in (a) and from the left and right in (b). A similar situation occurs for the vs.

This slight modification is important because now the us adjacent to the vertical boundaries (and similarly the vs adjacent to the horizontal boundaries) can be computed directly from the continuity equation. Furthermore, extrapolation is no longer needed because the us are located on the top and bottom boundaries (and the vs are located on the left and right boundaries).

The second and third shortcomings of scheme (a) apply to this scheme also.

(c) 4/1 *staggered grid*

On this grid, computation of the pressure boundary condition is not needed because no pressure is located on the boundary. Furthermore, while it appears to be staggered, the grid can be readily changed into a non-staggered one.

Consider the mass balance over element 'ne' shown in Figure 4. According to equation (8b), we write

$$p_{ne} = -\frac{1-\lambda}{2h\lambda}(u_{NE}+u_E-u_N-u_C+v_N+v_{NE}-v_C-v_E). \tag{14}$$

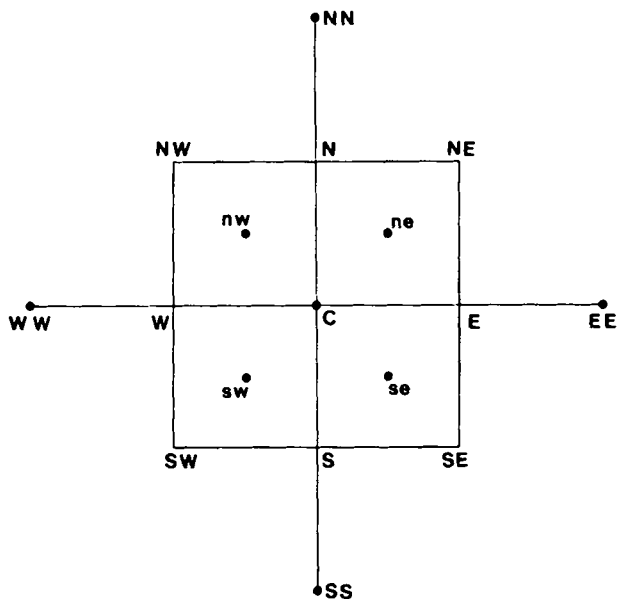

Figure 4. A grid showing the velocity components involved in the expression of the pressure gradient

Similar expressions can be written for p_{nw}, p_{sw} and p_{se} also. Consequently,

$$\left(\frac{\partial p}{\partial x}\right)_C = \frac{p_{ne}+p_{se}-p_{nw}-p_{sw}}{2h} = -\frac{1-\lambda}{4h^2\lambda}(2u_E+2u_W-4u_C+u_{NE}+u_{NW}-2u_N + u_{SE}+u_{SW}-2u_S+v_{NE}+v_{SW}-v_{NW}-v_{SE}). \tag{15}$$

If $u_{NE}=u_E=u_{SE}$, $u_N=u_C=u_S$ and $u_{NW}=u_W=u_{SW}$, then equation (15) reduces to

$$\left(\frac{\partial p}{\partial x}\right)_C = -\frac{1-\lambda}{h^2\lambda}(u_E-2u_C+u_W+v_{NE}+v_{SW}-v_{NW}-v_{SE}),$$

which is the finite difference discretization form of

$$\frac{\partial p}{\partial x} = -\frac{1-\lambda}{\lambda}\left(\frac{\partial^2 u}{\partial x^2}+\frac{\partial^2 v}{\partial x \partial y}\right). \tag{16}$$

Equation (15) reveals that the pressure gradient in this formulation can be expressed in terms of u and v at the nine grid points in the immediate vicinity of grid point C. This compactness cannot be achieved by other non-staggered grid formulations. For example, we can show that the pressure gradient for the 4/4 non-staggered grid is

$$\left(\frac{\partial p}{\partial x}\right)_C = \frac{p_E-p_W}{2h} = -\frac{1-\lambda}{4h^2\lambda}(u_{EE}+u_{WW}-2u_C+v_{NE}+n_{SW}-v_{NW}-v_{SE}), \tag{17}$$

which inevitably involves WW, SS, EE and NN grid points (when $(\partial p/\partial y)_c$ is also written).

Therefore we see that p can be completely disregarded throughout the 4/1 scheme. At every grid node ϕ now stands for u, v, $\partial p/\partial x$ and $\partial p/\partial y$. For 3D problems the unknowns will be u, v, w, $\partial p/\partial x$, $\partial p/\partial y$ and $\partial p/\partial z$. Added to the fact that no pressure boundary condition is needed, such a treatment greatly simplifies the computer programming and makes the 4/1 scheme quite attractive. Details of this treatment are described elsewhere.[24,25]

For most of the incompressible flow problems it is safe to assert that the discretization by the 4/1 scheme generally leads to a set of consistent algebraic equations. However, the set is slightly inconsistent for the present benchmark problem. For example, if we add up all the continuity equations that govern the circled ps shown in Figure 3(c) ($n=4$), the resulting algebraic equation becomes, according to equation (4),

$$0{\cdot}5(u_b-u_a)+0{\cdot}5(u_d-u_c)=0{\cdot}5(0{\cdot}56256-0)+0{\cdot}5(0{\cdot}56256-1)=0{\cdot}06256,$$

which should be zero if the algebraic system is consistent. Fortunately, this shortcoming does not appear to be serious because the inconsistent quantity will diminish as n increases (For example, it diminishes to 0·00012 for $n=32$).

When an iterative matrix solver is used, the solution can be considered as 'converged' when the residuals of all the discretized continuity equations become less than a non-zero (but small) constant.

When the algebraic system is consistent, the coefficient matrix of this scheme contains two zero eigenvalues, one associated with the hydrostatic pressure mode and the other with the checkerboard pressure mode.[11] Consequently, the pressure is oscillatory. However, this scheme has proved to be quite attractive despite these two shortcomings (see Table II).

(*d*) 4/5 *staggered grid*

As in scheme (c), all us and vs are located at the same grid points. Therefore, when the convection term is discretized, there is no need to take averages as required by schemes (a) and (b).

The diffusion term $\nabla^2\phi$ should be expressed in terms of the unknowns at the four corners of the control volume for the momentum balance. Referring to figure 3(d), we write

$$(\nabla^2\phi)_a = \frac{2}{h^2}(\phi_b + \phi_c + \phi_d + \phi_e - 4\phi_a)$$

instead of

$$(\nabla^2\phi)_a = \frac{1}{h^2}(\phi_f + \phi_g + \phi_h + \phi_i - 4\phi_a).$$

The computational domain will be covered twice if we draw all the control volumes for the mass balance, which suggests that two sets of the pressure solution are nearly unrelated. One set consists of *p*s located at the centre of each cell, and the other consists of *p*s located at the grid points.

As expected, programming of this scheme is relatively tedious, because each field variable needs two indexing systems.

(*e*) 5/4 *staggered grid*

This scheme is a slight modification of scheme (d). Two sets of pressure solutions also exist that are nearly unrelated. One set consists of *p*s located on vertical grid lines, and the other set consists of *p*s located on horizontal grid lines.

(*f*) 4/4 *non-staggered grid (with the continuity equation applied on the boundary to compute p there)*

We have found that, if the velocity components do not lie exactly on the face of the mass conservation control volume, multiple zero eigenvalues of the resulting coefficient matrix generally will exist.

In Figure 5, the velocity components do not lie at points w, s, e and n. Therefore u_e may be approximated by

$$u_e = a(u_7 + u_8) + b(u_3 + u_4 + u_{11} + u_{12}),$$

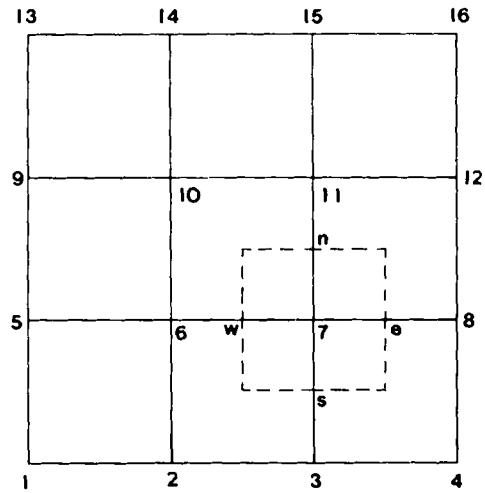

Figure 5. A 4/4 non-staggered grid

where a and b are weighting factors whose values depend on the scheme adopted (e.g. for schemes (f) and (g), $a=\frac{1}{2}$ and $b=0$; for the Galerkin finite element method with bilinear velocity and bilinear pressure square elements, $a=\frac{1}{3}$ and $b=\frac{1}{12}$).

The mass conservation over the control volume surrounding grid point 7 can be represented by

$$u_e-u_w+v_n-v_s=0$$

or

$$a(u_8-u_6+v_{11}-v_3)+b(u_{12}-u_{10}+u_4-u_2+v_{12}-v_4+v_{10}-v_2)=0.$$

Similarly, we can write the discretized equations at grid points 5, 13 and 15. When these equations are added up, we find that all the coefficients for the interior unknowns become zero; i.e.

$$0\times u_6+0\times u_{10}+0\times v_{10}+0\times v_{11}=\text{boundary terms},$$

which indicates that a zero eigenvalue is associated with such a linear combination of the discretized equations.

Discretization on the non-staggered 4/4 grid leads to oscillatory and erroneous pressure solutions. Sometimes this undesirable behaviour also manifests itself in the pressure gradient. As a simple example, we compute the classical lid-driven Stokes flow ($Re=0$) with the 4/4 scheme, and present the numerical results ($h=0{\cdot}1$) in Table IV. The validity of this solution can be readily checked by substituting the data point-by-point into the finite difference equation. For example, at $i=3$ and $j=3$ (for u or v, i or j varies from 1 to 11; for $\partial p/\partial y$, i or j varies from 2 to 10)

$$u_E-u_W+v_N-v_S=-0{\cdot}0396-0+0{\cdot}0396-0=0$$

and

$$\frac{1}{h^2}(v_W+v_S+v_E+v_N-4v_{ij})-\frac{\partial p}{\partial y}=(0{\cdot}0251+0+0{\cdot}0269+0{\cdot}0396$$
$$-4\times 0{\cdot}0301)/0{\cdot}01-(-2{\cdot}8828)=0.$$

We see from Table IV that the pressure gradient $\partial p/\partial y$ oscillates at least in the y-direction. It is believed that this behaviour is attributed to the inaccuracy of the scheme and may be unrelated to the contamination by pressure modes.

In this scheme it is inconvenient to replace the pressure with the pressure gradient as the field variable, because velocities beyond the nine-point stencil must be included in the expressions of the pressure gradient, as shown in equation (17).

(g) 4/4 non-staggered grid (with the momentum equation applied on the boundary to compute p there)

It is possible to eliminate the spurious oscillation in p by applying the momentum equation to compute the pressure boundary condition. By doing so, p_a and p_b in Figure 3(g) are directly linked in one equation such as

$$p_a=p_b+\frac{h}{Re}\left(\frac{\partial^2 u}{\partial x^2}\right)_a.$$

The major drawback of this scheme is that the mass conservation is poorly satisfied. In other words, the mass flow rates $\sum_{j=2}^{n} u(i,j)$ at each i are different from one another.

(h) 4/4 non-staggered grid (pressure Poisson equation)

Use of the pressure Poisson equation instead of the continuity equation has been accepted by CFD researchers for decades. However, we should note that the boundary condition of the

Table IV. The numerical solution of the lid-driven Stokes flow computed by using the 4/4 non-staggered grid (scheme (f))

					$u(i, j)$					
	$i=1$									$i=n+1$
$j=1$	1·0	1·0000	1·0000	1·0000	1·0000	1·0000	1·0000	1·0000	1·0000	1·0
	0·0	0·0000	0·2023	0·2598	0·3493	0·3427	0·3493	0·2598	0·2023	0·0000	0·0
	0·0	0·0000	0·0947	0·1467	0·1998	0·2063	0·1998	0·1467	0·0947	0·0000	0·0
	0·0	0·0000	−0·0581	−0·0649	−0·0619	−0·0643	0·0619	−0·0649	−0·0581	0·0000	0·0
	0·0	0·0000	−0·0311	−0·0456	−0·0530	−0·0556	−0·0530	−0·0456	−0·0311	0·0000	0·0
	0·0	0·0000	−0·0700	−0·0967	−0·1319	−0·1324	−0·1319	−0·0967	−0·0700	0·0000	0·0
	0·0	0·0000	−0·0386	−0·0615	−0·0863	−0·0895	−0·0863	−0·0615	−0·0386	0·0000	0·0
	0·0	0·0000	−0·0490	−0·0682	−0·1035	−0·1004	−0·1035	−0·0682	−0·0490	0·0000	0·0
	0·0	0·0000	−0·0249	−0·0396	−0·0605	−0·0612	−0·0605	−0·0396	−0·0249	0·0000	0·0
	0·0	0·0000	−0·0251	−0·0301	−0·0521	−0·0456	−0·0521	−0·0301	−0·0251	0·0000	0·0
$j=n+1$	0·0	0·0000	0·0000	0·0000	0·0000	0·0000	0·0000	0·0000	0·0000	0·0000	0·0
					$v(i, j)$					
	$i=1$									$i=n+1$
$j=1$	0·0	0·0000	0·0000	0·0000	0·0000	0·0000	0·0000	0·0000	0·0000	0·0000	0·0
	0·0	0·0000	0·0000	0·0000	0·0000	0·0000	0·0000	0·0000	0·0000	0·0000	0·0
	0·0	0·2023	0·2598	0·1470	0·0829	0·0000	−0·0829	−0·1470	−0·2598	−0·2023	0·0
	0·0	0·0947	0·1467	0·1052	0·0595	0·0000	−0·0595	−0·1052	−0·1467	−0·0947	0·0
	0·0	0·1442	0·1950	0·1432	0·0835	0·0000	−0·0835	−0·1432	−0·1950	−0·1442	0·0
	0·0	0·0636	0·1011	0·0833	0·0495	0·0000	−0·0495	−0·0833	−0·1011	−0·0636	0·0
	0·0	0·0742	0·0983	0·0814	0·0477	0·0000	−0·0477	−0·0814	−0·0983	−0·0742	0·0
	0·0	0·0249	0·0396	0·0356	0·0216	0·0000	−0·0216	−0·0356	−0·0396	−0·0249	0·0
	0·0	0·0251	0·0301	0·0269	0·0155	0·0000	−0·0155	−0·0269	−0·0301	−0·0251	0·0
	0·0	0·0000	0·0000	0·0000	0·0000	0·0000	0·0000	0·0000	0·0000	0·0000	0·0
$j=n+1$	0·0	0·0000	0·0000	0·0000	0·0000	0·0000	0·0000	0·0000	0·0000	0·0000	0·0
					$\partial p/\partial y(i, j)$					
		$i=2$								$i=n$
$j=2$		20·2262	25·9826	14·7004	8·2880	0·0000	−8·2880	−14·7004	−25·9826	−20·2262	
		−45·4545	−54·3309	−14·0151	−12·4980	0·0000	12·4980	14·0151	54·3309	45·4545	
		11·4439	6·7716	7·5865	3·3384	0·0000	−3·3384	−7·5865	−6·7716	−11·4439	
		−22·3484	−24·4588	−10·6060	−8·1593	0·0000	8·1593	10·6060	24·4588	22·3484	
		6·5188	3·5740	4·2017	1·6325	0·0000	−1·6325	−4·2017	−3·5740	−6·5188	
		−10·9848	−9·6944	−6·0606	−3·8396	0·0000	3·8396	6·0606	9·6944	10·9848	
		3·9110	3·0680	2·7015	1·2499	0·0000	−1·2499	−2·7015	−3·0680	−3·9110	
		−4·5454	−2·8828	−2·6515	−1·3445	0·0000	1·3445	2·6515	2·8828	4·5454	
$j=n$		2·5126	3·0114	2·6933	1·5491	0·0000	−1·5491	−2·6933	−3·0114	−2·5126	

pressure Poisson equation must be prescribed with great care to ensure the divergence-free condition. If the pressure boundary condition is obtained from the momentum equation, it is possible that the compressibility constraint will be violated. A simple illustration concerns a Stokes flow whose exact solution exists and is known to be

$$u(x, y)=\frac{x^3}{2}-\frac{xy^2}{2}, \qquad v(x, y)=\frac{x^2y}{2}-\frac{y^3}{2}, \qquad p(x, y)=x^2-y^2.$$

Such a flow is governed by

$$\nabla^2\mathbf{u}-\nabla p=0 \tag{18}$$

and

$$\nabla^2 p=0. \tag{19}$$

However, the solution violates the compressibility constraint because it can be readily shown that

$$\nabla\cdot\mathbf{u}=x^2-y^2\neq 0.$$

A comprehensive discussion on proper specification of the correct pressure boundary condition for the pressure Poisson equation is given by Gresho and Sani.[19]

(*i*) 4/4 *non-staggered grid (higher-order formulation)*

In this scheme the field variables are u, v, p, $\partial u/\partial x$, $\partial v/\partial y$, $\partial p/\partial x$ and $\partial p/\partial y$. For 3D flows the field variables become u, v, w, p, $\partial u/\partial x$, $\partial v/\partial y$, $\partial w/\partial z$, $\partial p/\partial x$, $\partial p/\partial y$ and $\partial p/\partial z$. Clearly, a large computer storage capacity is needed in this scheme. However, the accuracy of the numerical solution is impressively high, as can be seen in Table III.

The shortcomings of the nine schemes are summarized in Table II. We favour scheme (c) because it has the least shortcomings.

Table III presents the standard deviations of u, v and $\partial p/\partial y$ with respect to the exact solution for $Re=1$ and $Re=10$. Upwind difference is intentionally disregarded. If it had been used, inaccuracy associated with the artificial diffusion, added to that associated with the grid staggering, would have been introduced, making the assessment of the latter more difficult. Also, the difference between the conservative form and the non-conservative form is overlooked because the magnitude of convection considered here is small. These two latter subjects are reported elsewhere.

We observe the following facts from Table III:

(1) The accuracy of the staggered grid and non-staggered grid solutions appears to be comparable, except in schemes (a), (d) and (i).
(2) The accuracy of u and v at $Re=1$ is uniformly higher than that at $Re=10$. This trend is expected because the discretization of larger convection terms produces larger truncation errors.
(3) Scheme (i) is particularly accurate. We see that the standard deviations of its solution are one order of magnitude lower than those generated by other schemes. Even the solution at $Re=1$ computed on a 10×10 grid yields $e_u=0{\cdot}000518$, $e_v=0{\cdot}000524$ and $e_{py}=0{\cdot}080582$, which are more accurate than the results computed on a 20×20 grid by any of the other eight schemes.
(4) The accuracy of scheme (a) is very close to that of scheme (d), because scheme (d) is the superposition of (a) and (c), and only the nodal points used in scheme (a) are considered in calculating the standard deviations.
(5) The accuracies of schemes (a) and (d) rank second.

6. CONCLUDING REMARKS

A test problem, whose exact solution exists and is known, has been designed to systematically assess the accuracy and overall performance of nine finite difference schemes. Based on Tables II and III, we can make the following conclusions.

(a) Scheme (i) is significantly more accurate than the others if the comparison is restricted to the presented benchmark problem. In other words, the effect of grid staggering on the accuracy of the numerical solution is insignificant if the first derivatives $\partial u/\partial x$, $\partial v/\partial y$, $\partial p/\partial x$ and $\partial p/\partial y$ are computed by a scheme of higher-order accuracy instead of by the central finite difference method.

(b) If accuracy is not a major concern, the 4/1 staggered grid formulation appears attractive because of its simplicity. This scheme can be readily changed into a non-staggered grid scheme, and no pressure boundary condition is needed.

(c) The classical 2/1 staggered grid formulation of Harlow and Welch may be modified slightly to avoid extrapolations for the fictitious velocity components outside the boundary. The modification, however, leads to less accurate solutions.

ACKNOWLEDGEMENTS

This work is sponsored by DTNSRDC, Annapolis. The first author wishes to thank Dr. P. M. Gresho for enlightening technical communication during his sabbatical year at LLNL.

REFERENCES

1. F. H. Harlow and J. E. Welch, 'Numerical calculation of time-dependent viscous incompressible flow of fluid with free surface', *Phys. Fluids.* **8**, 2187–2189 (1965).
2. A. D. Gosman and F. J. K. Ideriah, 'Teach-T: a general computer program for two-dimensional, turbulent, recirculating flows', Department of Mechanical Engineering, Imperial College, London, 1976.
3. S. V. Patankar, *Numerical Heat Transfer and Fluid Flow*, Hemisphere, Washington, 1980, ch. 6.
4. H. H. Wong and G. D. Raithby, 'Improved finite-difference methods based on a critical evaluation of the approximation errors', *Numer. Heat Transfer*, **2**, 139–163 (1979).
5. T. M. Shih and A. L. Ren, 'Primitive-variable formulations using non-staggered grids', *Numer. Heat Transfer*, **7**, 413–428 (1984).
6. A. J. Chorin, 'Numerical solution of the Navier–Stokes equations', *Math. Comput.*, **22**, 745–762 (1968).
7. P. S. Huyakorn, C. Taylor, R. L. Lee and P. M. Gresho, 'A comparison of various mixed-interpolation finite elements in the velocity–pressure formulation of the Navier–Stokes equations', *Comput. Fluids*, **6**, 25–35 (1978).
8. C. P. Jackson and K. A. Cliffe, 'Mixed interpolation in primitive variable finite element formulations for incompressible flow', *Int. j. numer. methods eng.*, **17**, 1659–1688 (1981).
9. G. E. Schneider, G. D. Raithby and M. M. Yovanovich, 'Finite element solution procedures for solving the incompressible, Navier–Stokes equations using equal order variable interpolation', *Numer. Heat Transfer*, **1**, 433–451 (1978).
10. O. R. Burggraf, 'Analytical and numerical studies of the structure of steady separated flows', *J. Fluid Mech.*, **24**, 113–151 (1966).
11. R. Sani, P. Gresho, R. Lee, D. Griffiths and M. Engelman, 'The Cause and Cure(?) of the spurious pressures generated by certain FEM solutions of the incompressible Navier–Stokes equations', *Int. j. numer. methods fluids*, **1**, 17–43 (1981).
12. S. P. Vanka, B. C.-J. Chen and W. T. Sha, 'A semi-implicit calculation procedure for flows described in boundary-fitted coordinate systems', *Numer. Heat Transfer*, **3**, 1–19 (1980).
13. M. J. P. Cullen, 'Analysis of some low-order finite element schemes for the Navier–Stokes equations', *J. Comput. Phys.*, **51**, 273–290 (1983).
14. T. J. R. Hughes, W. K. Liu and A. Brooks, J. 'Finite element analysis of incompressible viscous flows by the penalty function formulation', *J. Comput. Phys.*, **30**, 1–30 (1979).
15. M. J. P. Cullen, 'Experiments with some low-order finite element schemes for the Navier–Stokes Equations', *J. Comput. Phys.*, **51**, 291–312 (1983).
16. W. E. Pracht, 'Calculating three-dimensional fluid flows at all speeds with an Eulerian–Lagrangian computing mesh', *J. Comput. Phys.*, **17**, 132–147 (1975).
17. P. M. Gresho and R. L. Lee, 'Partial vindication of the bilinear velocity, piecewise constant pressure element', *J. Comput. Phys.*, **60**, 161–164 (1985).

18. C. R. Maliska and G. D. Raithby, 'A method for computing three dimensional flows using non-orthogonal boundary-fitted coordinates', *Int. j. numer. methods fluids*, **4**, 519–537 (1984).
19. P. M. Gresho and R. L. Sani, 'On pressure boundary conditions for the incompressible Navier–Stokes equation', *Int. j. numer. methods fluids*, **7**, 1111–1145 (1987).
20. W. R. Briley, 'A numerical study of time-dependent rotation flow in a cylindrical container at low and moderate Reynolds number', *J. Comput. Phys.*, **14**, 20–35 (1974).
21. A. J. Chorin, 'A numerical method for solving incompressible viscous flow problems', *J. Comput. Phys.*, **2**, 12–26 (1967).
22. T. M. Shih and B. Hwang, 'Equivalence of the artificial compressibility method and the penalty function method, *Technical Report # DTRC-PAS-88-13*, 1988.
23. T. M. Shih, 'A procedure to debug computer programs', *Int. j. numer. methods eng.*, **21**, 1027–1037 (1985).
24. T. M. Shih and B. Hwang, 'Pressure gradient method for incompressible unsteady flows', *Technical Report # DTRC-PAS-88-12*, 1988.
25. C. H. Tan, 'A numerical scheme for solving incompressible Navier–Stokes equations', *Ph.D. dissertation*, the University of Maryland, 1988.